

## CAN THE LYMAN CONTINUUM LEAKED OUT OF H II REGIONS EXPLAIN DIFFUSE IONIZED GAS?

KWANG-IL SEON<sup>1</sup>

## Abstract

We present an attempt to explain the diffuse H $\alpha$  emission of a face-on galaxy M 51 with the “standard” photoionization model, in which the Lyman continuum (Lyc) escaping from H II regions propagates large distances into the diffuse interstellar medium (ISM). The diffuse H $\alpha$  emission of M 51 is analyzed using thin slab models and exponential disk models in the context of the “on-the-spot” approximation. The scale height of the ionized gas needed to explain the diffuse H $\alpha$  emission with the scenario is found to be of the order of  $\sim 1-2$  kpc, consistent with those of our Galaxy and edge-on galaxies. The model also provides a vertical profile, when the galaxy is viewed edge-on, consisting of two-exponential components. However, it is found that an incredibly low absorption coefficient of  $\kappa_0 \approx 0.4-0.8$  kpc<sup>-1</sup> at the galactic plane, or, equivalently, an effective cross-section as low as  $\sigma_{\text{eff}} \sim 10^{-5}$  of the photoionization cross-section at 912Å is required to allow the stellar Lyc photons to travel through the H I disk. Such a low absorption coefficient is out of accord with the properties of the ISM. Furthermore, we found that even the model that has the DIG phase only and no H I gas phase shows highly concentrated H $\alpha$  emissions around H II regions, and can account for only  $\lesssim 26\%$  of the H $\alpha$  luminosity of the DIG. This result places a strong constraint on the ionizing source of the DIG. We also report that the H $\alpha$  intensity distribution functions not only of the DIG, but also of H II regions in M 51, appear to be lognormal.

*Subject headings:* galaxies: individual: M 51 — galaxies: ISM — ISM: H II regions — ISM: structure

## 1. INTRODUCTION

Diffuse ionized gas (DIG) is a major component of the interstellar medium (ISM) in galaxies (Reynolds 1991; Walterbos & Braun 1996; Haffner et al. 2009). The large energy requirement of the DIG strongly suggests that OB stars are the only viable ionization source (Reynolds 1984). The “standard” photoionization model of the DIG assumes that the ionizing photons that leaked out of H II regions in the galactic disk ionize the diffuse ISM (Mathis 1986; Sokolowski & Bland-Hawthorn 1991; Domgörgen & Mathis 1994). If the Lyman continuum (Lyc, ionizing continuum) photons escaping from the traditional H II regions were the dominant source responsible for ionizing the DIG, then the H $\alpha$  intensity from the DIG would be expected to correlate with that of discrete H II regions. Ferguson et al. (1996) found a correlation between the DIG and bright H II regions over both small and large scales.

However, it is not clear how a major fraction of Lyc photons can escape from the immediate surroundings of an OB association and how the escaped photons can be transmitted across distances of the order of a kpc. Norman & Ikeuchi (1989) suggested that superbubbles or “chimneys” around OB associations could ionize the halo gas above the chimneys. Miller & Cox (1993), Dove & Shull (1994), and Dove, Shull, & Ferrara (2000) quantitatively investigated the possibility of penetration of the Lyc into the Galactic halo. These scenarios may explain the diffuse H $\alpha$  emission, in particular vertical H $\alpha$  filaments or “worms,” seen in external edge-on galaxies, such as NGC 891 (Rand, Kulkarni & Hester 1990; Dettmar 1990). However, the Lyc must travel not only large distances above the plane, but also within a galactic plane (Reynolds 1993). This requirement seems evident when the diffuse H $\alpha$  emission far from the classical H II regions in face-on galaxies are exam-

ined.

Zurita et al. (2002) were the first to attempt modeling the global morphology of the DIG of a face-on galaxy with the Lyc escaping from bright H II regions. They assumed a thin slab disk with a constant absorption coefficient over a galaxy NGC 157 and compared the predicted morphologies with the observed data by varying the absorption coefficient. In this way, they found that the diffuse H $\alpha$  surface brightness distribution is, surprisingly, well reproduced by assuming no significant absorption of ionizing photons.

However, they neither compared the absolute H $\alpha$  flux of the models with the observed data nor discussed the implications of the absorption coefficient obtained to explain the observed morphology. If OB stars are to provide the diffuse ionization, then the ISM must be not only transparent to ionizing photons, but also sufficiently dense to provide the observed H $\alpha$  emission (Miller & Cox 1993). In the extreme case of no absorption, no H $\alpha$  radiation is emitted. Therefore, it is necessary to compare the absolute H $\alpha$  flux as well as the morphology of the H $\alpha$  image. It is also worthwhile to consider a geometrically thick disk in the modeling and compare the scale height obtained to account for the observed H $\alpha$  luminosity with those of edge-on galaxies.

The transmission of the Lyc into the DIG has been attributed to the inhomogeneity of the ISM, such as a fractal H I distribution produced by ISM turbulence (Elmegreen 1997; Wood & Mathis 2004). However, no attempt has been made to quantify the ISM density structure required to allow the transmission of the Lyc. It is not clear whether such inhomogeneity of the ISM in typical spiral galaxies is consistent with the requirement of the “photoionization” scenario. Meanwhile, it is known that the probability distribution functions (PDFs) of not only the local densities, but also the column densities of the turbulent ISM, are lognormal (Vázquez-Semadeni 1994; Ostriker, Stone, & Gammie 2001; Fischera & Dopita 2004). With this property, it is possible to quantitatively access how turbulent or porous the ISM should

<sup>1</sup> Korea Astronomy and Space Science Institute, Daejeon, Republic of Korea, 305-348; email: kiseon@kasi.re.kr

be for the stellar Ly $\alpha$  radiation to be responsible for the diffuse H $\alpha$  emission with the “standard” photoionization model or whether the absorption coefficient obtained in the modeling is in accord with the current knowledge of the ISM.

In this paper, we calculate thin slab models similar to those of Zurita et al. (2002) and more elaborated models incorporating an exponential disk for a face-on galaxy M 51. We find that the “standard” scenario requires absorption too unrealistically small to be believed, but the obtained scale-height of the galactic disk is consistent with those of edge-on galaxies. We also report that the PDFs of the H $\alpha$  intensities of the DIG and H II regions in the galaxy M 51 are lognormal.

## 2. H $\alpha$ DATA

For our purposes, a face-on galaxy is the best choice since we can easily identify H II regions, i.e., the ionizing source that is expected to be the dominant source. When an H $\alpha$  emission map is ready, the first step for the analysis is then to separate H II regions from the diffuse H $\alpha$  emission. To do so, we used an automated photometry procedure known as “HIIPhot,” described in Thilker, Braun, & Walterbos (2000), in which they applied the procedure to the H $\alpha$  data of M 51. Therefore, as a matter of convenience, we use the same H $\alpha$  data of M 51 as they did. Their publicly available data, provided together with the “HIIPhot” procedure, has the same angular resolution, but a slightly smaller field size than that of Thilker, Braun, & Walterbos (2000).

For the present analysis, we assumed a distance of 9.6 Mpc to M 51 (Sandage & Tammann 1974). At this distance, a pixel in the image corresponds to a linear resolution of  $\Delta r = 32$  pc. No correction was attempted for extinction to compare with earlier studies. We detected 1356 H II regions. Of the total sample, 1061 regions were classified as “photometric-quality” detections having S/N  $\geq 5$ . The extent of each H II region was determined using a terminal surface brightness slope of 1.5 EM pc $^{-1}$ , as in Thilker, Braun, & Walterbos (2000). Here, EM is an emission measure (cm $^{-6}$  pc). A continuum-subtracted H $\alpha$  image, where H II regions were masked, and the H $\alpha$  intensity histograms for the DIG and H II regions are shown in Figure 1. It is evident in the figure that the H $\alpha$  intensity histograms are lognormal, both in the DIG and H II regions. The width of the lognormal distribution determines the porosity of the medium and is essential to the analysis of the transmission of the Ly $\alpha$ . The fit results will be used for the modeling of the DIG and discussed in later sections.

## 3. MODELS

### 3.1. Basic Assumptions

We employed the “on-the-spot” approximation, in which ionizing photons emitted by recombinations to the ground state of hydrogen in the ionized gas are assumed to be reabsorbed very close to their point of origination. However, strictly speaking, the approximation may not be applicable to the optically thin case that is the primary concern of the present study. The probability of a photon being remitted as an ionizing photon is the ratio of the recombination coefficient to the ground state of hydrogen ( $\alpha_1$ ) and that to all levels ( $\alpha_A$ ). The ratio is 0.33–0.43 for a gas in a temperature range of 5000–20,000 K (Osterbrock & Ferland 2006). This portion of the diffuse ionizing photons may escape the system or be reabsorbed elsewhere in the system. Therefore, the “on-the-spot” approximation would overestimate the total H $\alpha$  intensity by a factor of  $\lesssim 2$  in the optically thin case. The H $\alpha$

morphology would also be probably twice sharper than that of a more accurate calculation. These two limitations should be kept in mind when interpreting our results.

The purpose of this study is to simulate the situation in which the neutral hydrogen gas has a vertical scale height of  $h$ , and a density structure that can be described by an absorption coefficient  $\kappa(z)$  in the global sense so that some of the neutral hydrogen is ionized by the Ly $\alpha$  radiation. Since we assume that the Ly $\alpha$  photons absorbed in a volume are balanced by the immediate recombination, the H $\alpha$  surface brightness at each pixel is directly proportional to the absorbed number of Ly $\alpha$  photons within the volume and is independent of the unresolved cloud density structure, such as clumpiness or porosity. The amounts of Ly $\alpha$  intensities, which are emitted from all H II regions and absorbed at a point in the DIG, are co-added to calculate the H $\alpha$  intensity at the point.

### 3.2. Thin Slab Models

We first calculated two-dimensional thin slab models using the method described in Zurita et al. (2002), not only in order to compare our results with theirs, but also to obtain basic ideas on the parameter ranges needed to calculate more elaborated models. The H I layer in the galactic disk is assumed to be a thin slab of a constant thickness  $\Delta H = 2h$  and to have a constant absorption coefficient  $\kappa$  (kpc $^{-1}$ ). We took an average H I scale height of  $h = 100$  pc. We calculated the total radiation field absorbed within a volume  $\Delta V = (\Delta r)^2 \Delta H$  corresponding to a pixel of the H $\alpha$  image of the face-on galaxy. Here,  $(\Delta r)^2$  is the area corresponding to a pixel in the image, and the area of the volume subtended by the source  $\Delta A = \Delta H \Delta r$ . Because of geometrical dilution and absorption, the transmitted flux of stellar radiation at distance  $r$  from a source is  $L_0 e^{-\tau} / 4\pi r^2$ , where  $L_0$  is the total number of ionizing photons emitted per second at the source, and the optical depth  $\tau = \int \kappa dr$ . The stellar luminosity absorbed over volume  $\Delta V$  after traveling the optical depth  $\tau$  is then given by  $e^{-\tau} \Delta \tau L_0 (\Delta A / 4\pi r^2)$ , or, in general,  $e^{-\tau} (1 - e^{-\Delta \tau}) L_0 (\Delta A / 4\pi r^2)$ , where  $\Delta \tau = \kappa \Delta r$ .

Various absorption coefficients are examined to account for the effect of density inhomogeneity. We consider each pixel of H II regions as a point source with the effective Ly $\alpha$  luminosity equal to that corresponding to its measured H $\alpha$  intensity. Given a constant absorption coefficient  $\kappa$ , we obtain the H $\alpha$  surface brightness at pixel  $i$ :

$$I_i^{\text{DIG}} = \sum_j \frac{f_{\text{scale}} I_j^{\text{HII}}}{4\pi r_{ij}^2} \exp(-\kappa r_{ij}) \Delta A (1 - e^{-\kappa \Delta r}),$$

where  $f_{\text{scale}}$  is the ratio of the total luminosity of DIG to that of H II regions. A large fraction of the total H $\alpha$  emission (DIG + H II regions),  $\sim 0.5$ , is contributed by DIG, implying that the total Ly $\alpha$  luminosity emitted from the sources is about twice higher than that absorbed in H II regions. The luminosities from the DIG and H II regions are then approximately equal to each other ( $f_{\text{scale}} \approx 1$ ). Here,  $r_{ij}$  is the distance from a source pixel  $j$  to the pixel  $i$ , and  $\tau_{ij} = \kappa r_{ij}$  is the optical depth along the path from the pixel  $i$  to  $j$ . The conversion factors, the Ly $\alpha$  to H $\alpha$  luminosity and the luminosity to flux, are canceled out on both sides of the equation.

It should be noted here that Zurita et al. (2002) ignored the factor  $\Delta A (1 - e^{-\kappa \Delta r})$ . The effect of the factor  $1 - e^{-\kappa \Delta r}$  ( $\approx \kappa \Delta r$  as  $\kappa \Delta r \ll 1$ ) is to lower the amount of produced H $\alpha$  emission as the medium becomes increasingly transparent to

the Lyc. The  $H\alpha$  brightness increases with the disk thickness  $\Delta H$ . The factor  $f_{\text{scale}}$  is allowed to vary to take into account a larger scale height as well as to match the observed data, although it is initially meant to be the ratio of Lyc leakage toward DIG to that absorbed in H II regions. In other words, the scale height needed to be in accord with the observed data is  $h \approx 0.1 f_{\text{scale}}$  kpc. In this way, the scale height of the galaxy can be inferred.

We have varied the effective absorption coefficient from  $\kappa = 10^{-3}$  to  $10^2$   $\text{kpc}^{-1}$ . Typical results are shown in Figure 2. The scaling factors, defined by  $f_{\text{scale}} \equiv \sum I_{\text{data}} / \sum I_{\text{model}}$ , were multiplied to the models to match the overall  $H\alpha$  brightness level. We also show the intensity distributions of the model, observed data in the second row, and correlation plots between the model and observed flux in the form of two-dimensional histograms in the third row.

We note that, at the optically thin limit of  $\kappa \lesssim 0.1$   $\text{kpc}^{-1}$ , as the attenuation factor  $e^{-\kappa r} \approx 1$  for a system size of  $\sim 10$  kpc, the morphologies of the models are basically the same as in the case of no absorption ( $\kappa = 0$ ) and are determined by the geometrical dilution only. In the limit, however, we obtain much lower  $H\alpha$  intensity than the observed data although the overall morphology seems, at first glance, to resemble the observed image. The model and observed intensities are, in a general sense, linearly proportional to each other, as shown for  $\kappa \approx 0.1$   $\text{kpc}^{-1}$  in the third row of Figure 2. However, the model images are a bit broader near H II regions than the observed image, as also noted by Zurita et al. (2002). As  $\kappa$  increases, the overall morphology begins to deviate from the observed one. For large absorption coefficients (e.g., for  $\kappa = 3.16$   $\text{kpc}^{-1}$ ), the  $H\alpha$  emissions are mostly concentrated near H II regions. The correlation between the model and observed data also begins to deviate from the linear proportionality, as can be noted in third row of Figure 2. We, therefore, fitted the correlation between the observed and model intensities with a power-law  $I_{\text{data}} = f_{\text{scale}}^* (I_{\text{model}})^\beta$ .

The results are shown in Figure 3, together with  $f_{\text{scale}}$ . The third row of Figure 2 shows the best fit curves in red as well as the one-to-one curves in blue. In Figure 3(b), the slope  $\beta$  is a little smaller than 1 even at  $\kappa \ll 0.1$   $\text{kpc}^{-1}$ . It is also shown that the slope  $\beta$  decreases rapidly with increasing  $\kappa$  as  $\kappa \gtrsim 0.1$ , implying that the observed morphology cannot be reproduced well in this range because of fast attenuation of the Lyc while it is being propagated into the diffuse ISM. However, when the correlation histograms are compared with blue one-to-one curves, it is found that the correlation slope is close to 1 up to  $\kappa = 0.2$   $\text{kpc}^{-2}$ . Meanwhile, in the limit of  $\kappa \lesssim 0.1$   $\text{kpc}^{-1}$ , the scale factor increases with decreasing  $\kappa$ , as shown in Figure 3(a). Therefore, the optimal solution is obtained with  $\kappa \approx 0.1 - 0.2$   $\text{kpc}^{-1}$ . We also note that large scaling factors of  $\sim 13 - 22$  are required for these values, implying  $h \sim 1 - 2$  kpc for the generally accepted Lyc leakage fraction of  $\sim 0.5$ . The required scale height would be  $\sim 1 - 4$  kpc, considering that the present results may be overestimated by up to a factor of 2. These values are too large to be reconciled with the H I disk scale height, but consistent with the DIG scale heights of  $\sim 1 - 3$  kpc, measured from our Galaxy and external edge-on galaxies (e.g., Reynolds 1989; Rand 1996; Collins & Rand 2001).

A serious problem encountered in the present results is an extremely low absorption coefficient. Assuming the same H I column density of  $N_{\text{HI}} = 8.6 \times 10^{20}$   $\text{cm}^{-2}$  through the galactic disk of  $h = 100$  pc as Zurita et al. (2002), we obtain the ef-

fective cross-section  $\sigma_{\text{eff}} = \kappa / (N_{\text{HI}} / \Delta H) = 2.3 \times 10^{-23} (\kappa / 0.1 \text{ kpc}^{-1}) \text{ cm}^2$ . Zurita et al. (2002) obtained the best approximation to the morphology of the observed DIG surface brightness with  $\sigma_{\text{eff}} = 5.3 \times 10^{-23}$   $\text{cm}^2$ . This value corresponds to  $\kappa = 0.2$   $\text{kpc}^{-1}$ , consistent with our result of  $\kappa \approx 0.1 - 0.2$   $\text{kpc}^{-1}$ . Assuming a smaller column density of  $N_{\text{HI}} = 10^{20}$   $\text{cm}^{-2}$ , we obtain  $\sigma_{\text{eff}} = 2 \times 10^{-22} (\kappa / 0.1 \text{ kpc}^{-1}) \text{ cm}^2$ . These cross-sections imply virtually no absorption of the Lyc, i.e., as low as  $\sim 10^{-6} - 10^{-5}$  of the photoionization cross-section  $6.4 \times 10^{-18}$   $\text{cm}^2$  at  $912 \text{ \AA}$  (Verner & Yakovlev 1995). We also note that  $\sigma_{\text{eff}}$  is even lower than the dust extinction cross-section of  $2.3 \times 10^{-21}$   $\text{cm}^2 / \text{H}$  at  $912 \text{ \AA}$  (Draine 2003).

### 3.3. Exponential Disk Models

For exponential disk models, we employ a three-dimensional Monte Carlo radiation transfer code (Wood & Reynolds 1999) that was originally developed for the simulation of dust-scattering. A modified version has been used in the radiative transfer models of dust-scattering in the Ophiuchus region (Lee et al. 2008). The code was modified to simulate photoionization in the context of the ‘‘on-the-spot’’ approximation. Lyc photons are emitted from point source H II regions, as in thin slab models. We tracked the propagation of the Lyc photons from sources as they were absorbed and reemitted as  $H\alpha$  photons. The absorbed photon was 100% reemitted isotropically as  $H\alpha$  photon in the present simulations, while in dust-scattering simulations the photon was reemitted with a probability of  $0 < a < 1$  toward a new direction determined by a Henyey-Greenstein scattering phase function. In other words, our simulations were performed by assuming the albedo  $a = 1$ , asymmetry factor  $g = 0$ , and a single scattering. The reemitted  $H\alpha$  traveled toward the observer and was added into the  $H\alpha$  image. Absorption coefficients in each density grid were calculated assuming an exponential function,  $\kappa(z) = \kappa_0 \exp(-|z|/h)$ , where the absorption coefficient  $\kappa_0$  ( $\text{kpc}^{-1}$ ) at the galactic plane and the vertical scale height  $h$  are varied.

We first confirmed that the Monte Carlo models with  $h \ll 1$  kpc are consistent with the above thin slab models, and their total  $H\alpha$  intensities increase linearly with the scale height. At an optical thin limit of  $\kappa_0 \ll 1$   $\text{kpc}^{-1}$ , the morphologies of the models are basically the same as the case of no absorption ( $\kappa_0 = 0$ ), just as in thin slab models. Sample models are shown in Figure 4, together with the intensity distributions of the models, observed data in the second row, and correlation plots in the third row. The scaling factors, defined by  $f_{\text{scale}} \equiv \sum I_{\text{data}} / \sum I_{\text{model}}$ , were multiplied by the models to match the overall  $H\alpha$  brightness. Unlike thin slab models, the total  $H\alpha$  intensity is saturated at  $h \sim 1/\kappa_0$  as the scale height increases since the amounts of ionizing photons at high  $|z|$  declines rapidly and the  $H\alpha$  emission is dominated by the contributions from low  $|z| \lesssim 1/\kappa_0$ . Therefore, the scaling factor  $f_{\text{scale}}$  saturates as  $h$  increases. The trend is shown in Figure 5 for the models with  $\kappa_0 = 0.4$ , and  $10.8$   $\text{kpc}^{-1}$ . As  $\kappa_0$  increases, the  $H\alpha$  morphology becomes strongly concentrated near the H II regions, and the intensity distribution becomes wider as its low-intensity side is elongated. The elongation of the low-intensity side of the intensity histogram is shown in the blue curve of Figure 4(d), in which no  $f_{\text{scale}}$  was multiplied. For a given absorption coefficient, the morphological coincidence of the thick disk models with the observation is better than that of the thin slab models, as the  $H\alpha$  emission

from the thick disk models are from more extended regions. In other words, the intensity distribution is narrower than that for the thin slab models. This can be easily noticed by comparing the model of  $\kappa_0 = 1 \text{ kpc}^{-1}$  in Figure 2 and that of  $\kappa_0 = 2 \text{ kpc}^{-1}$  in Figure 4. Even with a higher absorption coefficient, the thick disk model is less concentrated near the H II regions than the thin slab model. As for thin slab models, we fitted the correlation between the observed and model intensities with a power-law and plotted the best fit curves in red lines and one-to-one curves in blue lines in the third row of Figure 4. We found that the models with  $\kappa_0 = 0.4\text{--}0.8 \text{ kpc}^{-1}$  predict the observed data nicely, and the scale height required to explain total H $\alpha$  intensity is  $\sim 1\text{--}2 \text{ kpc}^{-1}$ .

The problem of the extremely low absorption rate remains unsolved with the exponential disk models, although four times higher  $\kappa_0$  are obtained. Assuming the same H I column density over 0.1 kpc, as for the thin slab models, we obtained the effective absorption cross-section  $\sigma_{\text{eff}} = (0.9\text{--}1.9) \times 10^{-22} \text{ cm}^2$ , as low as  $\sim 10^{-5}$  of the photoionization cross-section. The obtained scale height is consistent with that from thin slab models. We note again that the scale height would be  $\sim 1\text{--}4 \text{ kpc}$ , considering that the present results may be overestimated by up to a factor of 2.

#### 4. OPACITY OF THE TURBULENT ISM TO THE LYC

We now examine whether such a small attenuation coefficient obtained in §3 is in accord with the current knowledge on the ISM density structure. What we measure from observation is the average column density  $\langle N \rangle$  or optical depth  $\langle \tau \rangle$  because of the finite spatial resolution. In the turbulent medium showing the lognormal nature of column density, the effective optical depth that the radiation field suffers, given an average optical depth  $\langle \tau \rangle$ , can be calculated by

$$\tau_{\text{eff}} = -\ln \int e^{-\tau} P(\ln \tau) d \ln \tau,$$

where the lognormal distribution is

$$P(\ln \tau) = \frac{1}{\sqrt{2\pi}\sigma_{\ln \tau}} \exp \left[ -\frac{(\ln \tau - \ln \tau_0)^2}{2\sigma_{\ln \tau}^2} \right]$$

(Fischera, Dopita, & Sutherland 2003). Here,  $\langle \ln \tau \rangle \equiv \ln \tau_0$  and  $\sigma_{\ln \tau}$  are the mean value and the standard deviation in logarithmic space. The mean values in linear and logarithmic scales are related by  $\ln \tau_0 = \ln \langle \tau \rangle - \sigma_{\ln \tau}^2/2$ , where  $\langle \tau \rangle$  is the mean in the linear scale. The relative standard deviation (contrast) in the linear scale,  $\sigma_{\tau}/\langle \tau \rangle = \sigma_{\tau/\langle \tau \rangle}$ , is related to the standard deviation in the logarithmic scale by  $\sigma_{\tau/\langle \tau \rangle}^2 = \exp(\sigma_{\ln \tau}^2) - 1$ . The relative deviation of optical depth  $\sigma_{\tau/\langle \tau \rangle}$  is always smaller than the density contrast  $\sigma_{\rho/\langle \rho \rangle}$ , as the accumulation of the density along a path length would average out the density contrast (Fischera & Dopita 2004). Given the observational or theoretical value of the column density contrast  $\sigma_{\tau/\langle \tau \rangle}$ , we can, then, obtain the lognormal distribution that describes the column density, and estimate the effective optical depth,  $\tau_{\text{eff}}$ , of the Lyc using these relationships.

Observationally, the turbulent ISM has been usually investigated by a power-law fit to the power spectra of the observable quantities proportional to column densities. The power-law indexes have been observed to be  $\gamma \approx -2.4 \sim -3.7$  from the warm and cold ISMs in our Galaxy and the Small Magellanic Cloud (Armstrong, Cordes, & Rickett 1981;

Crovisier & Dickey 1983; Schlegel, Finkbeiner, & Davis 1998; Stanimirovic et al. 2000; Miville-Deschênes et al. 2007). The power-law indexes can be related to the density contrast  $\sigma_{\rho/\langle \rho \rangle}$  by combining two relationships between the Mach number  $M$  and  $\gamma$ , and between  $M$  and  $\sigma_{\rho/\langle \rho \rangle}$ . We combine the numerical results of Kim & Ryu (2005), Kritsuk, Norman, & Padoan (2006), and Padoan et al. (2004), and find a relation between the Mach number and the power-law index of the density power spectrum,

$$\gamma = (-3.81 \pm 0.07)M^{(-0.16 \pm 0.01)},$$

as shown in Figure 6. From this, we estimate  $M \approx 1\text{--}12$  for the observed  $\gamma$ . Fischera, Dopita, & Sutherland (2003) found that the empirical reddening law for starburst galaxies is consistent with  $M \approx 1.3\text{--}22$ . Padoan, Jones, & Nordlund (1997) found that  $\sigma_{\rho/\langle \rho \rangle} \approx 0.5M$  through numerical simulations. We then obtain the upper limit on the column density contrast of  $\sigma_{\tau/\langle \tau \rangle} \leq \sigma_{\rho/\langle \rho \rangle} \approx 0.5\text{--}11$ . In Figure 7, we show  $\tau_{\text{eff}}$  as a function of  $\sigma_{\tau/\langle \tau \rangle}$  for various  $\langle \tau \rangle$ .

Although, in real situations, the H I column density is an order of  $\sim 10^{20}\text{--}10^{21} \text{ cm}^{-2}$  over 0.1 kpc scale, we calculate the effective optical depths for various column densities to demonstrate how small an absorption coefficient is required by the ‘‘standard’’ photoionization scenario. Assuming H I column densities of  $N_{\text{HI}} = 10^{20}$ ,  $10^{19}$ , and  $10^{18} \text{ cm}^{-2}$  over 0.1 kpc, we have  $\langle \tau \rangle = N_{\text{HI}}\sigma_{\text{photo}}$  ( $1 \text{ kpc}/0.1 \text{ kpc}$ )  $\sim 64,000$ ,  $6400$ , and  $640$  over a distance of 1 kpc, respectively. We then obtain effective absorption coefficients of  $\kappa_{\text{eff}} \gtrsim 11\text{--}159$ ,  $6.2\text{--}92$ , and  $3.5\text{--}45 \text{ kpc}^{-1}$  from Figure 7, for  $\sigma_{\tau/\langle \tau \rangle} \approx 0.5\text{--}11$ . Note that these values are the lower limits for various H I column densities, but are still much larger, by several orders of magnitude, than the  $\kappa_0 \approx 0.4\text{--}0.8 \text{ kpc}^{-1}$  required to account for the DIG by the ‘‘standard’’ photoionization model.

Recently, Miville-Deschênes & Martin (2007) found that  $\sigma_{\rho/\langle \rho \rangle} \sim 0.8$  for the warm neutral medium based on the kinematic H I observation. Hill et al. (2008) showed for the first time that the H $\alpha$  intensity PDF of our Galaxy is well represented by a lognormal distribution and found that  $M = 1.3\text{--}2.4$  through comparison with the turbulence simulations. We performed the same fit, as shown in Figure 1(b) and obtained a width of the lognormal distribution,  $\sigma_{\ln I} \sim 0.36 \pm 0.03 \text{ dex}$ ,  $\sim 1.5$  times wider than that of our Galaxy. We obtain  $M \lesssim 6.5\text{--}7.3$  for the DIG of M 51 by comparing the result with Table 1 in Hill et al. (2008). Assuming  $M = 8$  and  $\sigma_{\tau/\langle \tau \rangle} \approx 4$ , we have much stronger constraints on the absorption coefficient of  $\kappa_{\text{eff}} \gtrsim 19.3$ ,  $10.8$ , and  $6.1 \text{ kpc}^{-1}$  for  $N_{\text{HI}} = 10^{20}$ ,  $10^{19}$ , and  $10^{18} \text{ cm}^{-2}$  over 0.1 kpc, respectively.

The models calculated with these absorption coefficients yield H $\alpha$  morphologies significantly different from the observed one. This implies that the Lyc photons leaked from the H II regions are immediately absorbed by the diffuse ISM, even if it has escaped out of the H II regions. For comparison, we calculated the Mach numbers required to have the effective absorption coefficient  $\kappa = 0.8 \text{ kpc}^{-1}$ , assuming that the same relation between the standard deviation of column density and the Mach number is still valid in this extreme case:  $M > 2.0 \times 10^5$ ,  $1.8 \times 10^4$ , and  $1.6 \times 10^3$  for the media having  $N_{\text{HI}} = 10^{20}$ ,  $10^{19}$ , and  $10^{18} \text{ cm}^{-2}$  over 0.1 kpc, respectively.

## 5. DISCUSSION

### 5.1. Vertical Profile

By comparing the  $H\alpha$  emission data with models, we found that the vertical scale height of the face-on galaxy M 51 must be  $\sim 1-2$  kpc. Even though this value is obtained from the problematic absorption coefficient, we note that the scale height is consistent with the results not only from our Galaxy, but also from external edge-on galaxies (Reynolds 1989; Rand 1996; Collins & Rand 2001). It might also be noteworthy to examine how the galaxy M 51 may look when the galaxy is viewed edge-on. In Figure 8, we show the  $H\alpha$  map, assuming  $\kappa_0 = 0.4 \text{ kpc}^{-1}$  and  $h = 1.5$  kpc, which are expected when the galaxy is viewed edge-on, and the vertical profile of  $H\alpha$  image. The vertical profile of the model with the  $\kappa_0 = 0.4 \text{ kpc}^{-1}$  and  $h = 1.0$  kpc are shown as well for comparison. The  $H\alpha$  intensity from H II regions are not shown in the figure.

It is surprising that the simulated vertical  $H\alpha$  profile can be represented by a function consisting of two or more-exponential components. Observationally, the profile might be recognized by two-exponential components because of low surface brightness at high  $|z|$ . If the Ly $\alpha$  photons travel only perpendicularly to the galactic disk, the  $H\alpha$  profile would have the same scale-height as that of the exponential disk. However, the  $H\alpha$  radiation observed at a point with vertical height  $z$  consists of the contributions from the Ly $\alpha$  photons that have traveled longer distances, i.e.,  $(r^2 + z^2)^{1/2} > |z|$ , where  $r$  is the projected distance onto the galactic plane from the Ly $\alpha$  source. Therefore, the  $H\alpha$  intensity declines faster than that naively expected from the assumed vertical height of the exponential disk. The smaller the vertical distance, the more important the effect becomes. Beyond the height corresponding to the system size  $\sim 10$  kpc, the vertical profile converges to that of the disk, as the distances traveled by the Ly $\alpha$  become close to the vertical height, i.e.,  $(r^2 + z^2)^{1/2} \approx |z|$ . The trend is noticeable in Figure 8(b). We then have a vertical profile that resembles two-exponential components, within a few kpc. The profiles in Figure 8(b) are fitted with  $0.19e^{-z/1.1} + 0.33e^{-z/0.32}$  for  $h = 1.5$  kpc, and  $0.23e^{-z/0.80} + 0.32e^{-z/0.26}$  for  $h = 1.0$  kpc, and the fit profiles are denoted by diamonds. We have masked the regions at  $|z| < 0.3$  kpc in fitting the vertical profile to minimize the effect due to the assumption that the H II regions are located in the galactic plane ( $z = 0$ ). The vertical height of the smaller exponential component is expected to depend not only on the vertical profile of H I gas, but also of the details of the vertical extents of the H II regions.

The  $H\alpha$  vertical emission profiles of edge-on galaxies are known to be well represented by two exponential components (Rand 1997; Miller & Veilleux 2003a). Wang, Heckman, & Lehnert (1997) identified the two components kinematically through the observation of face-on galaxies, including M 51, a “quiescent” DIG with a high ionization state and small scale height (few hundred pc), and a “disturbed” DIG with a high ionization state and moderate scale height (0.5–1 kpc). The origin and evolution of the extended, or extraplanar, DIG seen in edge-on galaxies are not clear, but two alternatives are generally considered (e.g., Heald et al. 2006, 2007). The gas is generally considered to participate in a star formation-driven disk-halo flow, such as that described in the fountain or chimney models (Shapiro & Field 1976; Norman & Ikeuchi 1989). Alternatively, the gas could have been accreted from the intergalactic medium or from companion galaxies (e.g., van der Hulst & Sancisi 2005). The vertical structure seen in our models seems to support the star formation-related origin of the extraplanar DIG. However,

without kinematical information, as was used in Heald et al. (2006, 2007), it is not easy to examine the two-components predicted in these models with  $\kappa = 0.4 \text{ kpc}^{-1}$  do correspond to the kinematically identified components, and/or to determine how much of the DIG is associated with the quiescent component and how much is contained in extended disturbed layers. In fact, it is not only surprising, but also very puzzling, that the models with a problematic absorption rate predicts not only the apparent morphologies of M 51, but also the two exponential components seen in edge-on galaxies.

## 5.2. Density Structure of the ISM

As suggested by numerical simulations (e.g., Vázquez-Semadeni 1994; Kim & Ryu 2005), the density distribution of turbulently disturbed ISM is represented by a lognormal distribution, of which the width depends on how the medium is turbulent. Padoan, Jones, & Nordlund (1997) found that the observational result of Lada et al. (1994), which was that the variation of the stellar extinction in dark clouds correlates with the mean extinction, is consistent with the lognormal distribution of the dust density. Wada, Spaans, & Kim (2000) showed that the luminosity function of the H I column density in the Large Magellanic Cloud is lognormal. More recently, Hill et al. (2008) found that the  $H\alpha$  emission measure perpendicular to the Galactic plane from the DIG in the Milky Way is well fitted by a lognormal distribution, with a standard deviation of  $\sigma_{\ln I} \sim 0.2$  dex. Berkhuijsen & Fletcher (2008) showed that the PDFs of the average density, not only of the DIG, but also of the H I gas in our Galaxy, are close to lognormal, with a standard deviation  $\sigma_{\langle n \rangle} \sim 0.3$  dex. In Figure 1(b), we showed that the PDFs of the  $H\alpha$  intensity, i.e., emission measures, from the DIG and H II regions in M 51 are well-represented by a lognormal function. The standard deviation obtained from the DIG in M 51 is a bit higher than those of our Galaxy.

Wang, Heckman, & Lehnert (1997) studied kinematics of the DIG in M 51, together with other galaxies and found that the DIG is more disturbed kinematically than the gas in the giant H II regions. We, thus, compare the widths of  $H\alpha$  intensity distributions of the DIG and H II regions in Figure 1(b) and found no significant difference between them, except an extended tail toward low intensities shown in the DIG only. However, it is unclear whether the extended tail might be related to the more disturbed component seen by Wang, Heckman, & Lehnert (1997).

In §4, we found that an unrealistically small absorption, even smaller than dust-extinction, is necessary to explain the global features of the DIG with the Ly $\alpha$  leakage from the H II regions. The turbulent ISM with lognormal density PDF can be much more transparent to the Ly $\alpha$ , up to an order of  $1 \sim 3$  depending on the width of the PDF, compared to homogeneous ISM, as shown in Figure 7. However, such a small attenuation found here cannot be reconciled with these values, as discussed in §4. In addition, the attenuation rate is not consistent even with the dust optical depth of  $\tau_{\text{dust}} \sim 13$  at  $912\text{\AA}$  ( $A_V \sim 3$ ) obtained by comparing  $H\alpha$  and  $\text{Pa}\alpha$  emissions measured toward the H II regions of M 51 (Quillen & Yukita 2001; Scoville et al. 2001). Such large amounts of dust surrounding H II regions should absorb Ly $\alpha$  photons immediately in the vicinities of the H II regions.

Radiative transfer models have been successful in explaining the dust scattering and absorption for our Galaxy and external galaxies with reasonable amounts of dust, consis-

tent with the observed amounts of interstellar dust (e.g., Schiminovich et al. 2001; Bianchi 2007). Unless the topology of the interstellar dust and neutral hydrogen are completely different and decoupled from each other, the radiative transfer of the Ly $\alpha$  should not differ significantly from that expected from observed amounts of neutral hydrogen. In their study of dust scattering in clumpy media, Witt & Gordon (1996) showed that the effective optical depth of a system is mainly determined by the covering factor, i.e., the fraction of  $4\pi$  steradian of a solid angle filled by clumps as seen by the source rather than by the individual optical depth of clumps. The transmission of the Ly $\alpha$  is also mainly determined by the covering factor of dilute regions seen by the source. Such a large covering factor of low density regions may be achieved by fountain flow or chimneys around OB associations (Shapiro & Field 1976; Norman & Ikeuchi 1989). Filaments seen in edge-on galaxies may originate from the star formation-driven structures. Meanwhile, Rossa et al. (2004) presented high spatial resolution (5 pc) observations of the extraplanar DIG in the edge-on galaxy NGC 891 and found no clear broadening of the filamentary structures toward high  $|z|$  expected from individual chimneys. They, therefore, concluded that the chimney scenario is most likely not responsible for the gas and energy transport into the halo. In addition, Wang, Heckman, & Lehnert (1997) found that M 51 has a pronounced “diffuse” H $\alpha$  emission based on its high value of mean/rms of the H $\alpha$  surface brightness. Dove, Shull, & Ferrara (2000) showed that the dense swept up shell of material by the dynamical action of supernovae and stellar winds would trap ionization photons within superbubbles. Given the diffuseness or smoothness of the H $\alpha$  emission and the approximate equality of H $\alpha$  luminosities of the DIG and H II regions, the ISM should have an extremely unrealistic configuration, completely evacuated straight thin holes extending over the order of 1 kpc, randomly covering  $\sim 1/2$  of the  $4\pi$  solid angle seen by the sources.

The atomic ISM may be divided into two phases, except the hot gas of temperature  $\sim 10^6$  K: the neutral hydrogen gas (or clouds) and the DIG (or interclouds) phases. Our aim was to investigate the situation in which the stellar Ly $\alpha$  radiation propagates into the “initially” neutral ISM, ionize some portion of the gas, and maintain two phases. Since the ISM is not fully ionized, the H I gas prevents the propagation of the Ly $\alpha$  photons to maintain the ionization state of the DIG. However, it would be worthwhile to imagine an ISM in which the H I gas phase has no effect on the propagation of the stellar Ly $\alpha$  photons and the freely transmitted Ly $\alpha$  radiation maintains the ionization state of the DIG. In other words, assume that the H I gas phase is completely evacuated somehow, and the DIG is left alone. Then, the radiative transfer in the medium will be determined by the observed property of the DIG that is deduced from the H $\alpha$  intensity distribution in §4. Adopting  $M = 8$ ,  $\sigma_{\tau/(\tau)} = 4$  from the DIG of M 51, and  $N_{\text{HI}} \sim 1 \times 10^{20} \text{ cm}^{-2}$  over  $\sim 1$  kpc estimated in the Galactic plane (Reynolds 1991), the effective absorption coefficient is  $\sim 10.8 \text{ kpc}^{-1}$ . The model for these parameters is shown in Figure 4(d). The model shows a highly concentrated H $\alpha$  profile near the H II regions and predicts only about  $1/f_{\text{scale}} \sim 26\%$  of the observed H $\alpha$  luminosity. Since the relative deviation of the column density is an upper limit, the amount of H $\alpha$  that can be produced in this medium is even smaller, i.e.,  $\lesssim 26\%$ . A more stringent constraint would be obtained, assuming a Mach number of  $M \sim 1.2 - 2.4$  esti-

mated from our Galaxy (Hill et al. 2008). Therefore, the OB associations in the H II regions are not likely to be a main source in ionizing the DIG. The only way to resolve this problem would be to assume alternative ionizing sources outside of H II regions, in-situ of the DIG. If this is the case, the similarity in the H $\alpha$  morphologies between the models and the observational data may be a coincidence.

## 6. CONCLUDING REMARKS

We investigated whether the global features of the DIG can be explained in the context of the “standard” photoionization model. The most important result of this study is that we quantified the topology or “porosity” of the ISM required by the “standard” photoionization scenario in the contexts of the lognormal PDF. We found that even without the H I gas phase, the DIG phase cannot be maintained by the stellar Ly $\alpha$  radiation alone, implying that main ionizing source is not the OB associations in the H II regions. Since the Ly $\alpha$  that leaked out of the H II regions can account for, at most, only  $\lesssim 26\%$  of the H $\alpha$  luminosity of the DIG, the alternative sources should play a significant role in ionizing the DIG, especially in the inter-arm regions. Even with the morphological coincidence of the Ly $\alpha$  leakage models with the H $\alpha$  data, we cannot rule out the possibility that alternative ionizing sources are generally correlated with star formations and, thus, with the H II regions, as various gas and dust components are well correlated with each other, and the sources are playing a significant role in ionizing the DIG. The strong correlation between the DIG and H II regions does not necessarily indicate the direct association of the DIG with the H II regions.

Other authors have arrived at similar conclusions, both in terms of producing the amount of ionized gas observed and in producing the observed spectral signature of the DIG, that alternative sources other than hot stars in the H II regions are needed in heating and/or ionizing the DIG. Rand, Kulkarni & Hester (1990) estimated that the total energy input by chimneys into the halo to account for the DIG of NGC 891, a galaxy that in many ways is very similar to our own, is a factor 10–20 higher than the estimates for our Galaxy. Although the supernova rate is likely to be a few times higher than in our Galaxy, the required superbubble formation rate was inconsistent with the observations.

The emission-line ratios of the DIG are significantly different from those of typical H II regions. In the DIG, [Si II]  $\lambda 6716/\text{H}\alpha$  and [N II]  $\lambda 6583/\text{H}\alpha$  are enhanced relative to the H II regions (Haffner, Reynolds, & Tufte 1999; Ferguson, Wyse, & Gallagher 1996; Rand 1997; Greenawalt et al. 1998; Collins & Rand 2001; Hoopes & Walterbos 2003; Voges & Walterbos 2006). The pure photoionization models in diluted media predict the enhancement very well. However, the models predict that the ratio [Si II]/[N II] should increase with  $z$ , in contrast to the observations that the ratio versus the distance from the H II regions remains nearly constant in the DIG (Haffner, Reynolds, & Tufte 1999; Collins & Rand 2001). The behaviors of these low ionization lines can be explained by the gas temperature increase alone, without having a secondary source of ionization (Haffner, Reynolds, & Tufte 1999). On the other hand, the ratio [O III]  $\lambda 5007/\text{H}\alpha$  cannot be fully explained by a temperature increase alone (Collins & Rand 2001). According the “standard” photoionization scenario, the ratio [O III]/H $\alpha$  should decrease with  $z$  or the distance from the H II regions in a photoionization scenario. However, the opposite trend or the

relative constant with  $z$  is seen not only in edge-on galaxies (Rand 1998; Collins & Rand 2001), but also in face-on galaxies including M 51 (Wang, Heckman, & Lehnert 1997; Hoopes & Walterbos 2003; Voges & Walterbos 2006). One possible way to explain this high line ratio is to assume a secondary ionization source that contributes a small but increasing fraction of the  $H\alpha$  with  $z$ . Collins & Rand (2001) explored the possibility that ionization by shocks (Shull & McKee 1979) or turbulent mixing layers (Slavin, Shull, & Begelman 1993) is responsible for some of the DIG emission of the edge-on galaxies NGC 4302 and UGC 10288. They found that the composite models, of which up to  $\sim 16$ –45% of the  $H\alpha$  arises from shocks, better reproduce the variations of line ratios than the photoionization models alone, although no model reproduces the line ratios to within the errors. Similar conclusions were obtained for other edge-on galaxies by Rand (1998) and Miller & Veilleux (2003b). Hoopes & Walterbos (2003) tested the feasibility of “leaky H II region” models, in which the transmitted ionizing continua of density-bounded H II regions power the DIG, and concluded that other ionization or heating mechanisms play a role in ionizing the DIG. In addition, the He I  $\lambda 5876/H\alpha$  line intensity ratio in the DIG of

our Galaxy is found to be significantly less than that observed in H II regions, challenging the O star ionization models (Reynolds & Tufté 1995).

Another scenario investigated by Hoopes & Walterbos (2000), Hoopes, Walterbos, & Bothun (2001) is that field OB stars ionize some of the DIG. They measured the  $H\alpha/FUV$  intensity ratios of ten spiral galaxies, and concluded that late OB stars in the field are indeed important ionization sources. However, Voges & Walterbos (2006) concluded that field star ionization models do not fit the data of M 33 well and that about 30% leakage from H II regions is necessary. Accretion from the intragalactic medium or companion galaxy would be an attractive alternative for the origin of, at least some of, the DIG. Heald et al. (2006, 2007) compared the kinematics of optical emission lines obtained from two edge-on galaxies NGC 891 and NGC 4302 with an ballistic model of a galactic fountain model (Collins, Benjamin, & Rand 2002) and found a strong disagreement between the observed kinematics and those predicted by the model. As they noted, galaxies may reside in halos populated by a various mixture of accreting gas and star formation-driven gas. However, further analyses are required to quantitatively estimate their contributions in ionizing the DIG.

## REFERENCES

- Armstrong, J. W., Cordes, J. M., & Rickett, B. J. 1981, *Nature*, 291, 561  
 Berkhuijsen, E. M., & Fletcher, A. 2008, *MNRAS*, 390, L19  
 Bianchi, S. 2007, *A&A*, 471, 765  
 Collins, J. A., & Rand, R. J. 2001, *ApJ*, 551, 57  
 Collins, J. A., Benjamin, R. A., & Rand, R. J. 2002, *ApJ*, 578, 48  
 Crovisier, J., & Dickey, J. M. 1983, *A&A*, 122, 282  
 Dettmar, R.-J. 1990, *A&A*, 232, L15  
 Draine, B. T. 2003, *ApJ*, 598, 1017  
 Domgörgen, H., & Mathis, J. S. 1994, *ApJ*, 428, 647  
 Dove, J. B., & Shull, J. M. 1994, *ApJ*, 430, 222  
 Dove, J. B., Shull, J. M., & Ferrara, A. 2000, *ApJ*, 531, 846  
 Elmegreen, B. G. 1997, *ApJ*, 477, 196  
 Ferguson, A. M. N., Wyse, R. F. G., Gallagher, J. S., Hunter, D. A. 1996, *AJ*, 111, 2265  
 Ferguson, A. M. N., Wyse, R. F. G., Gallagher, J. S. 1996, *AJ*, 112, 2567  
 Fischera, J., Dopita, M. A., & Sutherland, R. S. 2003, *ApJ*, 599, L21  
 Fischera, J., & Dopita, M. A. 2004, *ApJ*, 611, 919  
 Greenawalt, B., Walterbos, R. A. M., Thilker, D., & Hoopes, C. G. 1998, *ApJ*, 506, 135  
 Haffner, L. M., Reynolds, R. J., & Tufté, S. L. 1999, *ApJ*, 523, 223  
 Haffner, L. M., Dettmar, R.-J., Beckman, J. E., Wood, K., Slavin, J. D., Giammanco, C., Madsen, G. J., Zurita, A., Reynolds, R. J. 2009, accepted by *Reviews of Modern Physics*, 2009arXiv0901.0941H  
 Heald, G. H., Rand, R. J., Benjamin, R. A., Bershad, M. A. 2006, *ApJ*, 647, 1018  
 Heald, G. H., Rand, R. J., Benjamin, R. A., Bershad, M. A. 2007, *ApJ*, 663, 933  
 Hill, A. S., Benjamin, R. A., Kowal, G., Reynolds, R. J., Haffner, L. M., & Lazarian, A. 2008, *ApJ*, 686, 363  
 Hoopes, C. G., & Walterbos, R. A. M. 2000, *ApJ*, 541, 597  
 Hoopes, C. G., Walterbos, R. A. M., & Bothun, G. D. 2001, *ApJ*, 559, 878  
 Hoopes, C. G., & Walterbos, R. A. M. 2003, *ApJ*, 586, 902  
 Kim, J., & Ryu, D. 2005, *ApJ*, 630, L45  
 Kritsuk, A. G., Norman, M. L., & Padoan, P. 2006, *ApJ*, 638, L25  
 Lada, C. J., Lada, E. A., & Clemens, D. P., & Bally, J. 1994, *ApJ*, 427, 694  
 Lee, D.-H., Seon, K.-I., Min, K.-W., Park, Y.-S., Yuk, I.-S., Edelstein, J., Korpela, E. J., Sankrit, R., Park, S. J., & Ryu, K. S. 2008, *ApJ*, 686, 1155  
 Mathis, J. S. 1986, *ApJ*, 301, 423  
 Miller III, W. W., & Cox, D. P. 1993, *ApJ*, 417, 579  
 Miller, S. T., & Veilleux, S. 2003a, *ApJS*, 148, 383  
 Miller, S. T., & Veilleux, S. 2003b, *ApJ*, 592, 79  
 Miville-Deschênes, M.-A., & Martin, P. G. 2007, *A&A*, 469, 189  
 Miville-Deschênes, M.-A., Lagache, G., Boulanger, F., Puget, J.-L. 2007, *A&A*, 469, 595  
 Norman, C. A., & Ikeuchi, S. 1989, *ApJ*, 345, 372  
 Ostriker, E. C., Stone, J. M., & Gammie, C. F. 2001, *ApJ*, 546, 980  
 Osterbrock, D. E., & Ferland, G. J. 2006, *Astrophysics of Gaseous Nebulae and Active Galactic Nuclei*, 2nd ed. (Sausalito: University Science Books), 22  
 Padoan, P., Jones, B. J. T., & Nordlund, Å. 1997, *ApJ*, 474, 730  
 Padoan, P., Jimenez, R., Juvela, M., & Nordlund, Å. 2004, *ApJ*, 604, L49  
 Rand, R. J., Kulkarni, S. R., & Hester, J. J. 1990, *ApJ*, 352, L1  
 Rand, R. J. 1996, *ApJ*, 462, 712  
 Rand, R. J. 1997, *ApJ*, 474, 129  
 Rand, R. J. 1998, *ApJ*, 501, 137  
 Rossa, J., Dettmar, R.-J., Walterbos, R. A. M., & Norman, C. A. 2004, *AJ*, 128, 674  
 Quillen, A. C., & Yukita, M. 2001, *AJ*, 121, 2095  
 Reynolds, R. J. 1984, *ApJ*, 282, 191  
 Reynolds, R. J. 1989, *ApJ*, 339, L29  
 Reynolds, R. J. 1991, *IAUS*, 144, 67  
 Reynolds, R. J. 1993, *ASPC*, 35, 338  
 Reynolds, R. J., & Tufté, S. L. 1995, *ApJ*, 439, L17  
 Sandage, A., & Tammann, G. A. 1974, *ApJ*, 194, 559  
 Scoville, N. Z. et al. 2001, *ApJ*, 122, 3017  
 Schiminovich, D., Friedman, P. G., Martin, C., & Morrissey, P. F. 2001, *ApJ*, 563, L161  
 Schlegel, D. J., Finkbeiner, D. P., & Davis, M. 1998, *ApJ*, 500, 525  
 Shapiro, P. R., & Field, G. B. 1976, *ApJ*, 205, 762  
 Shull, J. M., & McKee, C. F. 1979, *ApJ*, 227, 131  
 Slavin, J. D., Shull, J. M., & Begelman, M. C. 1993, *ApJ*, 407, 83  
 Sokolowski, J., & Bland-Hawthorn, J. 1991, *PASP*, 103, 911  
 Stanimirovic, S. et al. 2000, *A&A*, 315, 791  
 Thilker, D. A., Braun, R., & Walterbos, R. A. M. 2000, *AJ*, 120, 3070  
 van der Hulst, J. M., & Sancisi, R. 2005, in *ASP Conf. Ser.* 331, Extra-Planar Gas (San Francisco: ASP), 139  
 Vázquez-Semadeni, E. 1994, *ApJ*, 423, 681  
 Verner, D. A., & Yakovlev, D. G. 1995, *A&AS*, 109, 125  
 Voges, E. S., & Walterbos, R. A. M. 2006, *ApJ*, 644, L29  
 Wada, K., Spaans, M., Kim, S. 2000, *ApJ*, 540, 797  
 Walterbos, R. A. M., & Braun, R. 1996, *ASPC*, 106, 1  
 Wang, J., Heckman, T. M., & Lehnert, M. D. 1997, *ApJ*, 491, 114  
 Witt, A. N., & Gordon, K. D. 1996, *ApJ*, 463, 681  
 Wood, K., & Reynolds, R. J. 1999, *ApJ*, 525, 799  
 Wood, K., & Mathis, J. S. 2004, *MNRAS*, 353, 1126  
 Zurita, A., Beckman, J. E., Rozas, M., & Ryder, S. 2002, *A&A*, 386, 801

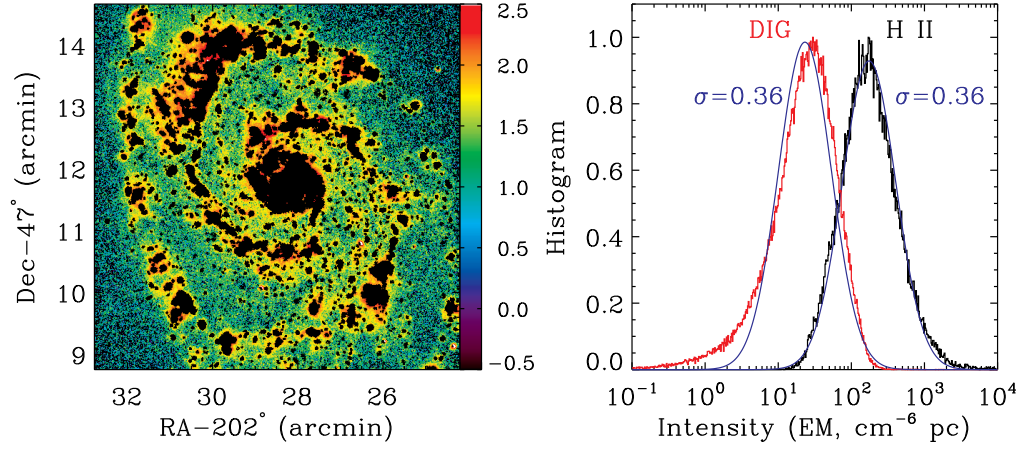


FIG. 1.— (a)  $H\alpha$  image of M 51 in logarithmic scale (EM,  $\text{cm}^{-6}$  pc). The H II regions were masked. (b) Histograms of  $H\alpha$  intensities for the DIG and H II regions. Blue curves denote the best-fit lognormal functions, as discussed in §4 and §5.

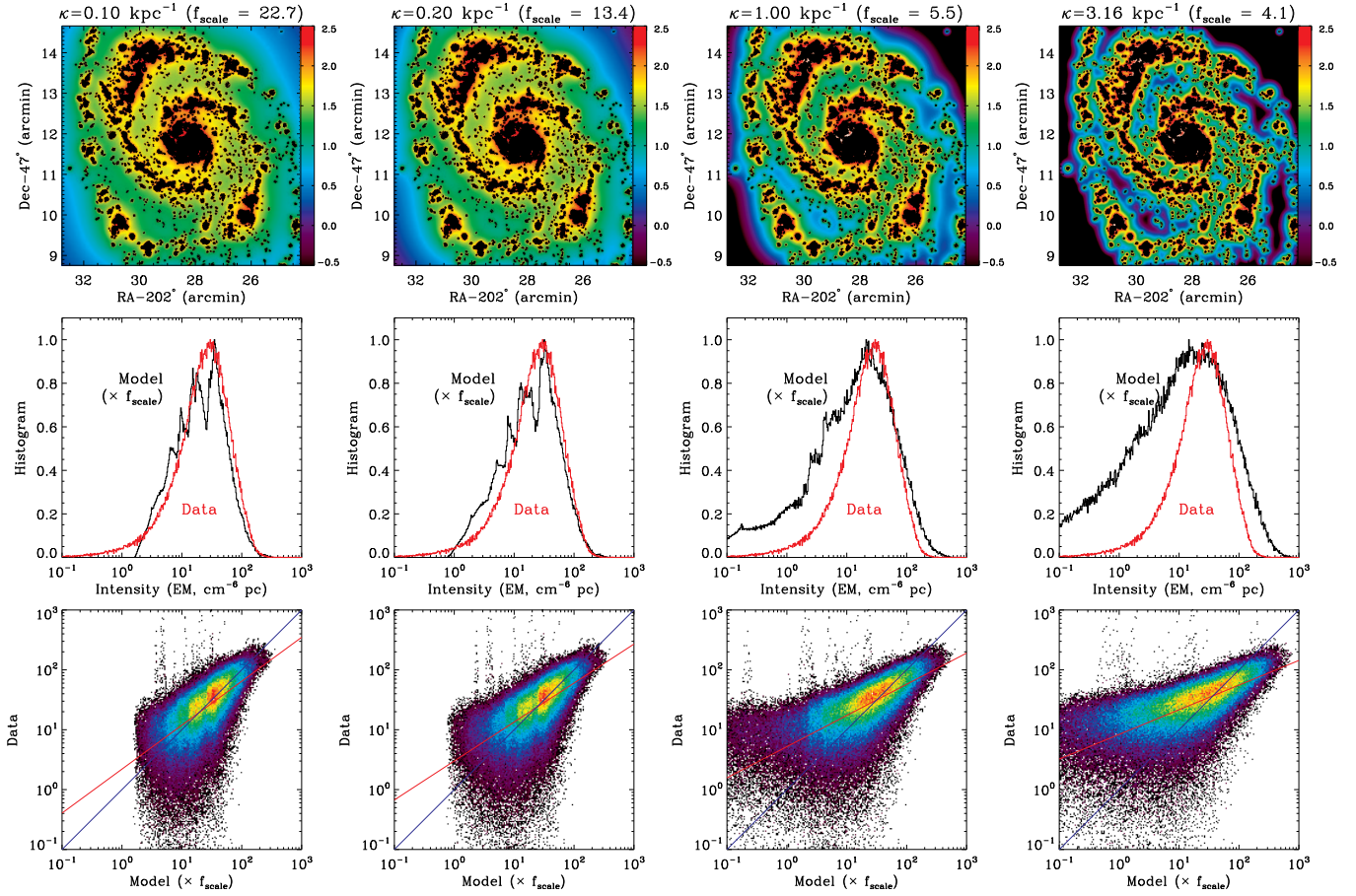


FIG. 2.— Thin slab models calculated for various absorption coefficients. Predicted model images with the same color scales as in Fig. 1, intensity histograms of the model and observed data, and correlation plots between the model and observed data are shown in the first, second, and third rows, respectively.

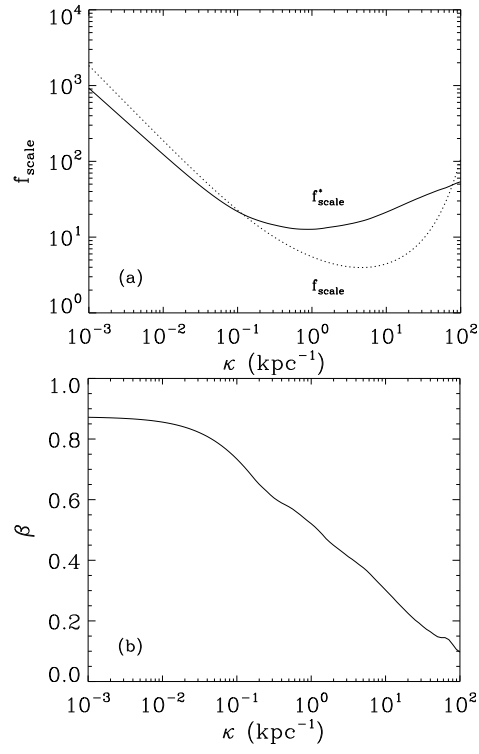


FIG. 3.— Best fit parameters with  $I_{\text{data}} = f_{\text{scale}}^* (I_{\text{model}})^\beta$ . The dotted line was obtained by  $f_{\text{scale}} = \sum I_{\text{data}} / \sum I_{\text{model}}$ .

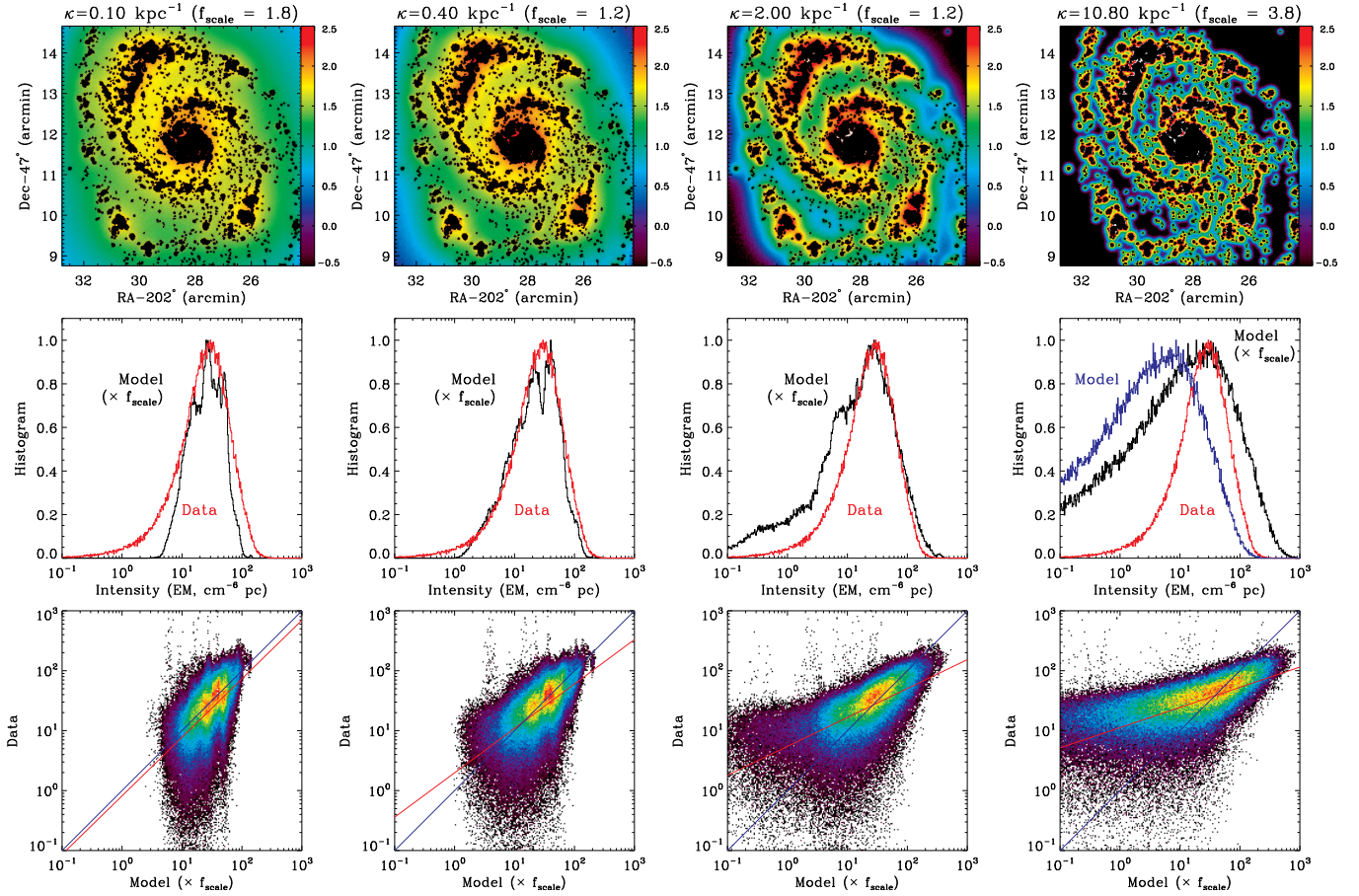


FIG. 4.— Exponential disk models calculated for various absorption coefficients and scale height: (a)  $\kappa_0 = 0.1 \text{ kpc}^{-1}$  and  $h = 3 \text{ kpc}$ , (b)  $\kappa_0 = 0.4 \text{ kpc}^{-1}$  and  $h = 1.5 \text{ kpc}$ , (c)  $\kappa_0 = 2.0 \text{ kpc}^{-1}$  and  $h = 1 \text{ kpc}$ , and (d)  $\kappa_0 = 10.8 \text{ kpc}^{-1}$  and  $h = 1 \text{ kpc}$ . Predicted model images with the same color scales as in Fig. 1, intensity histograms of the model and observed data, and correlation plots between the model and observed data are shown in the first, second, and third rows, respectively.

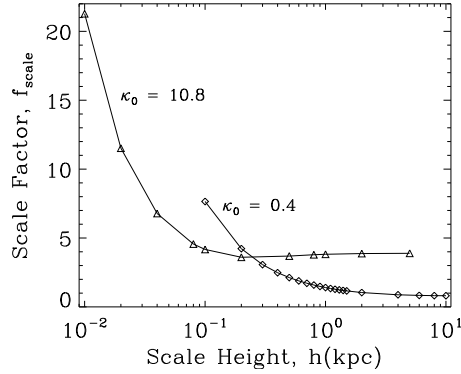


FIG. 5.— Variation of the scale factor,  $f_{\text{scale}} \equiv \sum I_{\text{data}} / \sum I_{\text{model}}$ , for the exponential disk model with the absorption coefficient  $\kappa_0 = 0.4 \text{ kpc}^{-1}$  and  $10.8 \text{ kpc}^{-1}$ .

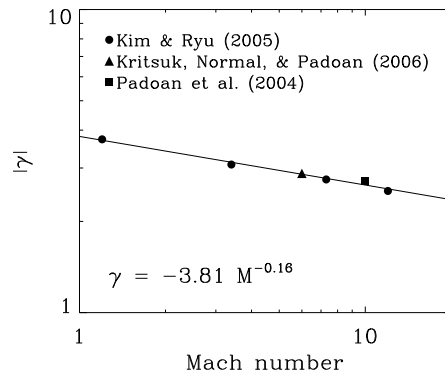


FIG. 6.— Power-law slope versus the Mach number from numerical simulations of the turbulent ISM, and the best-fit curve.

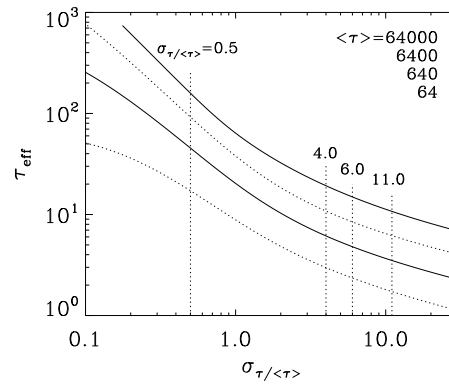


FIG. 7.— Effective optical depth versus the column density contrast for various average optical depths.

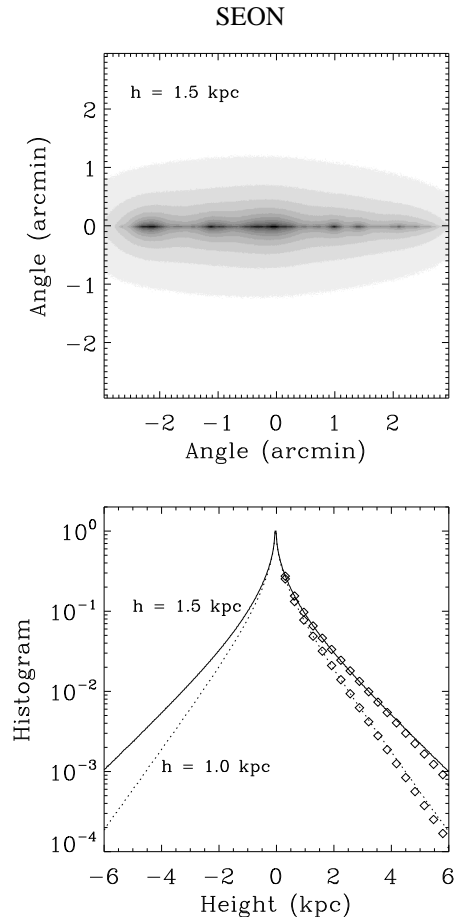


FIG. 8.— (a) Model for the galaxy M 51 when it is viewed edge-on, assuming  $\kappa_0 = 0.4 \text{ kpc}^{-1}$  and  $h = 1.5 \text{ kpc}$ , (b) the vertical profile of the H $\alpha$  intensity for two models:  $\kappa_0 = 0.4 \text{ kpc}^{-1}$ ,  $h = 1.5 \text{ kpc}$ ,  $\kappa_0 = 0.4 \text{ kpc}^{-1}$ , and  $h = 1.0 \text{ kpc}$ . Here, the diamond symbols denote two-exponential fits for  $|z| > 0.3 \text{ kpc}$ .